

Dynamic magnetization reversal in CoPt_3 dots: Magnetic force microscopy measurements at remanence

S. Boukari, J. Venuat, A. Carvalho, D. Spor, J. Arabski, and E. Beaurepaire

IPCMS, UMR 7504 CNRS-ULP, Boîte Postale 43, 23 rue du Loess, F-67034 Strasbourg Cedex 2, France

(Received 12 July 2007; revised manuscript received 9 January 2008; published 15 February 2008)

We have studied the magnetization reversal of $\text{Co}_{28}\text{Pt}_{72}$ single crystal dots down to $0.2\ \mu\text{m}$ diameter with perpendicular anisotropy under slow magnetic field sweep rates ($10^4\ \text{Oe/s}$) as well as with field pulses ($6.7 \times 10^{11}\ \text{Oe/s}$). The magnetic state of the dots in the remanent state is observed by magnetic force microscopy. After application of short field pulses, $1\ \mu\text{m}$ dots are frequently multidomain, whereas $0.2\ \mu\text{m}$ dots are always single domain. The nucleation volume is estimated either from aftereffect measurements or by fitting the increase of the dynamic coercive field versus field sweep rate. Its value amounts to a few $10^{-19}\ \text{cm}^3$. We show that the wall velocity around nucleation centers is larger than in the rest of the sample.

DOI: [10.1103/PhysRevB.77.054416](https://doi.org/10.1103/PhysRevB.77.054416)

PACS number(s): 75.40.Gb, 75.75.+a, 75.60.Ej

I. INTRODUCTION

Magnetization reversal dynamics in ferromagnetic thin films or small structures is an important issue, especially regarding patterned media with perpendicular magnetic anisotropy as a candidate to increase the bit density. With a data transfer rate close to the gigahertz range, the reversal of an individual bit should be carried out with a field pulse in the nanosecond time scale.

Magnetization reversal in ferromagnetic thin films occurs via nucleation and domain wall (DW) motion. Nucleation occurs by random switching of activation volumes, and the switching is thermally activated. DW motion takes place either by the thermally activated switching of an activation volume adjacent to existing domains or by viscous DW motion.^{1,2} Within this framework, several models were proposed to describe the magnetization reversal.^{3,4} In particular, they yield a relation between the coercive field and the field sweep rate. These models mainly differ in the form of the energy barrier that the activation volume has to overcome.⁵

In this work, we combine observations of magnetic domains and dynamic magnetization measurements in order to study the reversal of dots with perpendicular anisotropy upon applying nanosecond field pulses.

II. EXPERIMENTAL PROCEDURE

The samples were grown in an ultrahigh vacuum molecular beam epitaxy system. The (0001)-oriented sapphire substrate was first outgassed at $900\ ^\circ\text{C}$ for several hours. A Pt buffer layer of $11.5\ \text{nm}$ was then deposited at $900\ ^\circ\text{C}$. After lowering the sample temperature to $400\ ^\circ\text{C}$, Co and Pt were then co-evaporated at a flux of 0.0047 and $0.016\ \text{nm/s}$, respectively. The thickness of the alloy was $21.5\ \text{nm}$. The sample was finally capped with $2\ \text{nm}$ Pt to avoid any oxidation.

Electron-beam lithography was used to pattern the film into circular dots with diameter of either 1 , 0.5 , or $0.2\ \mu\text{m}$. The dots were arranged on a square lattice of $100 \times 100\ \mu\text{m}^2$ with a periodicity of $2\ \mu\text{m}$ for the 1 and $0.5\ \mu\text{m}$ dots, and $0.5\ \mu\text{m}$ for the $0.2\ \mu\text{m}$ dots. A copper microcoil was then created by lift-off on top of the array of dots such

that magnetic field pulses may be generated on the dots within the microcoil (Fig. 1).

This design, thus, forces the current to flow around a loop of $23\ \mu\text{m}$ internal diameter and $65\ \mu\text{m}$ external diameter. The current was driven through the coil by a homemade generator to produce field pulses of $\sim 230\ \text{Oe/A}$.⁶ The time for the current to pass from 10% to 90% of the peak value is $15\ \text{ns}$, almost independent of the peak value. The width at half maximum decreases from $24\ \text{ns}$ at $4.5\ \text{kOe}$ to $22\ \text{ns}$ at $12\ \text{kOe}$. The film was ion milled down to the sapphire substrate so as to isolate the dots from the microcoil. The magnetic hysteresis loops were recorded by magneto-optical Kerr effect (MOKE) and by superconducting quantum interference device (SQUID). The diameter of the area probed by the laser beam was $\approx 100\ \mu\text{m}$. Magnetic force microscopy (MFM) was used to image the remanent state of the dots.

III. RESULTS AND DISCUSSION

The epitaxial growth of the film was confirmed by *in situ* high energy electron diffraction. The crystalline parameter in the growth direction was determined by x-ray diffraction

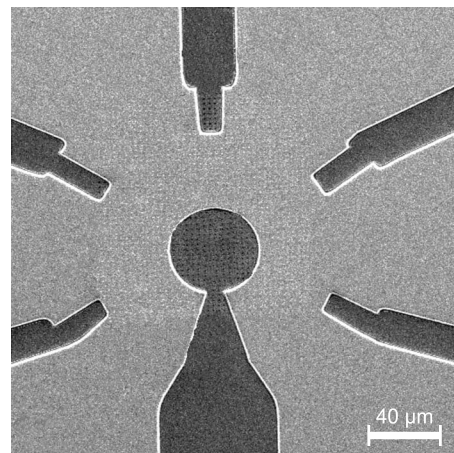


FIG. 1. Scanning electron microscope view of the copper microcoil after lift-off. The $100 \times 100\ \mu\text{m}^2$ array of dots is situated in the middle, but is hardly visible on this image.

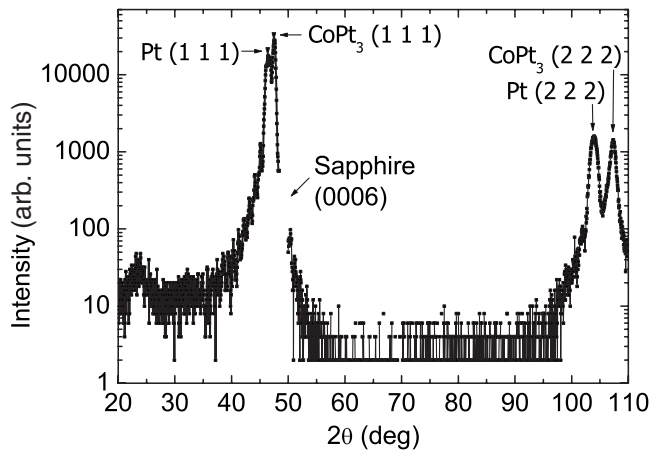


FIG. 2. X-ray diffraction intensity in the θ - 2θ geometry using Co K radiation ($\lambda=1.789$ Å).

(Fig. 2). From the intense diffraction peaks at 47.35° and 107.35° , we deduce a periodicity along the growth direction of 1.92 Å. This corresponds to the distance between the (111) planes of a disordered fcc $\text{Co}_x\text{Pt}_{1-x}$ alloy with a lattice parameter of 3.84 Å and x around 0.25 . The very low intensity of the peak characteristic of the $L1_2$ fcc ordered phase (around 23°) indicates that the alloy is chemically disordered. When compared to data on bulk disordered $\text{Co}_x\text{Pt}_{1-x}$ alloys,⁷ our 3.84 Å lattice parameter reflect 72% Pt and 28% Co concentrations. From the width of the (111) and (222) diffraction peaks, we deduce a coherence length of 22 nm, which is on the same order as the thickness of the film.

We present in Fig. 3 magnetic hysteresis loops obtained using a SQUID magnetometer with the field in-plane and perpendicular to the plane. The saturation magnetization M_s was found to be 340 emu/cm³. These loops are characteristic of a film with an easy magnetization axis that is perpendicular to the surface. Along the easy direction, the loop is almost square with 94% remanence and a coercive field of 2.4 kOe. From the area enclosed between the magnetization loops along the easy and hard axes, we deduce an effective anisotropy of 1.9×10^6 erg/cm³. The corresponding anisotropy

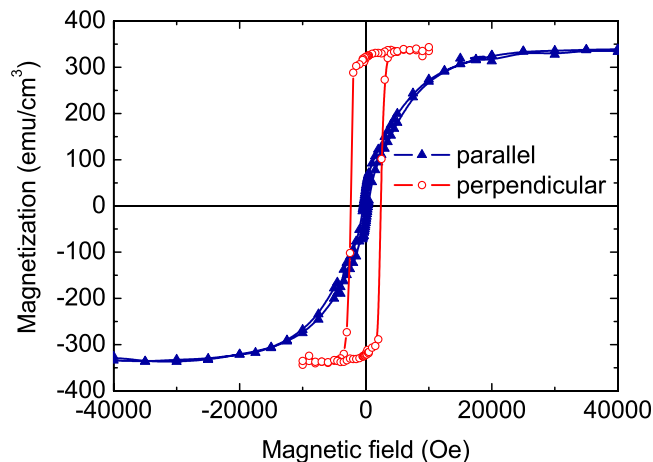


FIG. 3. (Color online) Hysteresis loops with the field parallel and perpendicular to the film plane.

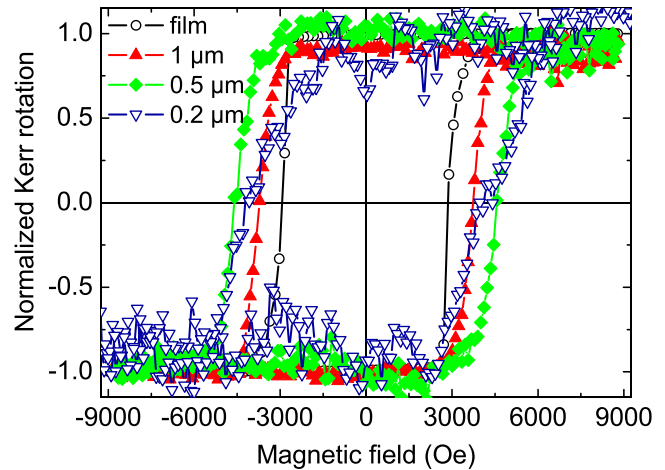


FIG. 4. (Color online) MOKE hysteresis loops for the film, and 1 and 0.2 μm dots.

field is 11.2 kOe. The observation of a perpendicular easy axis despite the lack of long-range ordering is in agreement with previous results obtained on $\text{Co}_x\text{Pt}_{1-x}$ alloys for which the anisotropy was attributed to short-range order.^{8,9}

We now present in Fig. 4 magnetic hysteresis loops obtained through MOKE. Note that the hysteresis loop of the film differs from the one recorded by SQUID magnetometry (Fig. 3). Indeed, the coercive field is larger (2.9 kOe) and the remanence is 100%. This difference is due to the faster field sweep rate in the magneto-optical measurements.¹⁰ A square shape for the hysteresis loop is related, for films with a high uniaxial anisotropy, to a magnetization reversal that begins at a few nucleation centers, followed by an expansion of these domains by DW propagation.¹¹ Since the coercive field is well above the Walker critical field $H_{crit}=2\alpha\pi M_s=256$ Oe in our case (with a damping parameter $\alpha=0.12$),¹² DW motion is not thermally activated but viscous, leading to a smooth shape for the DWs.^{2,13} Patterning the film leads to an increase in the coercive field, which reaches about the same value for the 0.5 and 0.2 μm dots. However, the magnetization reversal starts at about the same field value for both the continuous film and the arrays of dots. This shows that no extra low nucleation field site appears upon structuring the film. The observed increase in the field at which magnetization starts to decrease—to 11.6 kOe for the 1 μm dots and to 12.4 kOe for the 0.2 μm dots—likely reflects an increase in the effective anisotropy field due to shape effects.

To obtain insight into the reversal mechanism of the 1 μm dots, we then turned to magnetic field pulses. After saturating the magnetization, we first applied a 4.7 kOe magnetic field pulse and then imaged the resulting magnetic domain structure. Depending on the dot, we observe either no reversal or only one domain resulting from a nucleation event followed by DW propagation [Fig. 5(a)]. The average diameter of a domain created during a first pulse of 4.7 kOe is $d_1 \sim 150$ nm. A second pulse of the same amplitude was then applied to study the expansion of the magnetic domains that were created during the first pulse. Referring to Fig. 5(c), we observe that the domain size increased by DW propagation. We note that the size of the domains that were present before

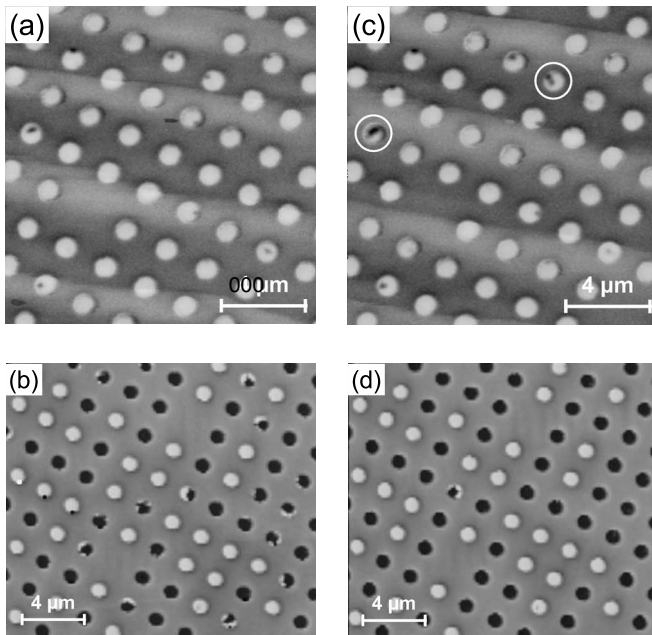


FIG. 5. MFM images of the domain structure for the 1 μm dots after (a) a first and (c) a second pulse of 4.7 kOe, and after (b) a first and (d) a second pulse of 10.5 kOe.

the application of the second pulse increased very little due to this second pulse: DW propagated over ~ 25 nm, such that the domains reached a mean diameter of $d_2 \sim 200$ nm. Aside from the expansion of the preexisting domains, there can also be new nucleation events. If a nucleation occurs close to a preexisting domain, it can lead, after the second pulse, to one domain with an elongated shape. This cannot be distinguished from the anisotropic expansion of one single domain. For the analysis, we therefore disregarded the two circled dots in Fig. 5(c).

The diameter of a domain after the first pulse is $d_1 = d_{nuc} + 2v_1\Delta t$, where d_{nuc} is the diameter of the initial nucleus and v_1 is the DW velocity during the first pulse of duration Δt . After an additional pulse, the diameter increases to $d_2 = d_1 + 2v_2\Delta t$, with v_2 the DW velocity during this pulse. If we assume that the DW velocity was the same during the first and second pulses, we may subtract 50 nm due to DW propagation from the 150 nm diameter of the domains after the first pulse to find an unusually huge nucleation volume of ~ 100 nm in diameter. In order to test the assumption of equal DW propagation speed during the first and second pulses and to explain why the domains increase so little during the second pulse, we will compare later on different models that are available in the literature to extract an upper limit for the nucleation volume.

Noting that the DW propagation velocity increases with field, we observe that, for a field pulse of amplitude 10.5 kOe, most of the dots for which a nucleation event occurred are almost completely reversed after the first pulse. Those that are not fully reversed during the first pulse are completely reversed after the second pulse.

Regarding the 0.2 μm dots, we were not able to observe any multidomain state: after one field pulse, there is either no reversal or a complete reversal (Fig. 6). We observed fully

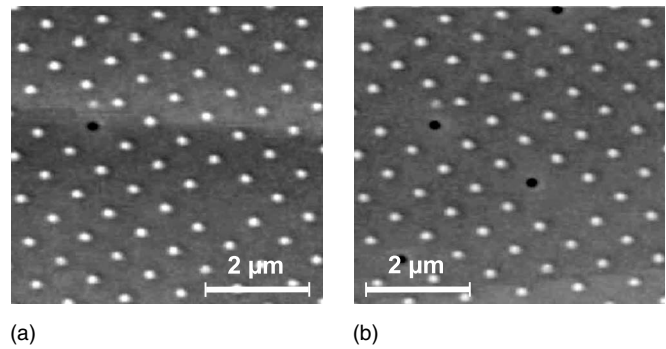


FIG. 6. MFM images of the domain state for the 0.2 μm dots after the application of one 8.5 kOe field pulse (left) and one 10.5 kOe field pulse (right).

reversed dots only after applying a field pulse as high as 8.5 kOe, in line with the higher anisotropy field of these dots. For such a field value, the DW propagation is fast enough to reverse a dot within the time duration of one field pulse.

The nucleation volume can be evaluated by magnetic aftereffect measurements: after saturating the magnetization, we measured, from the analysis of MFM images, the magnetization decrease as a function of time in a reversed field close to the coercive field.^{14,15} Following Jamet *et al.*,¹⁶ we define the time at which a proportion $\alpha = N(t)/N_s$ of the dots is reversed:

$$t_\alpha(H) = \tau_0 \exp\left(\frac{2M_s V_p^* H_{p,\alpha}}{kT}\right) \exp\left(\frac{-2M_s V_p^* H}{kT}\right).$$

$1/\tau_0$ is the attempt frequency, $H_{p,\alpha}$ is defined as $\int_0^{H_{p,\alpha}} f(H_p) dH_p = \alpha$, $f(H_p)$ is the activation field distribution, M_s is the saturation magnetization, and V_p is the activation volume. This model is strictly only valid for reversal by thermally activated DW propagation.^{10,16} Nevertheless, it provides a useful approximation in the case of reversal by nucleation and subsequent viscous wall motion, and it yields entirely analytical results (see hereafter for the validity of the approximation). Figure 7 shows the magnetic aftereffect measurements on the 0.2 μm dots. Since with our microcoil it is only possible to deliver short field pulses, the time window of several orders of magnitude was covered by applying a succession of field pulses. The proportion α was then calculated from MFM images at remanence by counting the number $N(t)$ of reversed dots. From $t_{0.17}$, we deduce an activation volume V_p^* of $(3 \pm 1) \times 10^{-19}$ cm³, and $(2.3 \pm 0.7) \times 10^{-19}$ cm³ from $t_{0.5}$. Assuming a cylindrical shape for the activation volume, its diameter is close to half the exchange length $\sqrt{A/2\pi M_s^2} = 7.8$ nm ($A = 0.43 \times 10^{-11}$ J/m is the exchange constant¹⁷).

We try now to evaluate the nucleation volume by fitting the evolution of the coercive field with field sweep rate within three different models: a moving DW model,³ a domain nucleation model,³ and a droplet model.⁴ These models mainly differ in the expression of the activation energy E_A as a function of magnetic field: $E_A = V_p^* M_s (H_p - H)$ for the propagation model, $E_A = V_n^* M_s (H_K - H)^2 / 2H_K$ for the nucle-

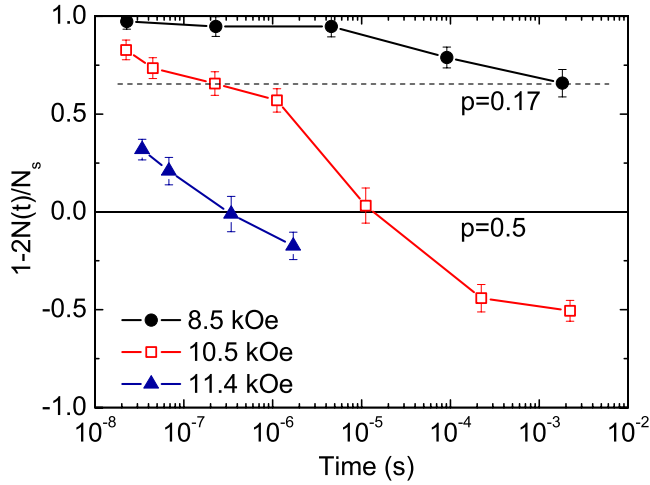


FIG. 7. (Color online) Normalized magnetization as a function of time for the $0.2 \mu\text{m}$ dots in different applied fields.

ation model, and $E_A = E_0(1/H - 1/\epsilon H_K)$ for the droplet model. In the above equations, V_p^* and V_n^* are magnetic reversal activation volumes, H_K is the anisotropy field, and ϵ is a reduction factor that accounts for the fact that nucleation occurs at spots with a reduced anisotropy.

The droplet model was introduced to explicitly account for the creation of a domain wall during the nucleation.⁴ Within this model, the minimum diameter for a reversed stable domain is $\gamma/HM_s = 22 \text{ nm}$ for $H = 4.7 \text{ kOe}$, where γ is the DW energy density. The activation energy involved in the nucleation model reduces to that of the moving wall model provided that the field is small with respect to the anisotropy field. It is, indeed, straightforward to show that we should then have $V_p^* = V_n^*$ and $H_p = H_K/2$. The model that we used to determine the activation volume from the magnetic aftereffect measurements assumes that the energy barrier is of the same form as the one involved in the moving DW model.

In Fig. 8, we present our experimental determination of the dynamic coercive field for two dot sizes as well as the best fits for the three models described above. The value of the coercive field for the low sweep rate was determined from hysteresis loops recorded by MOKE using an electromagnet. The value at high sweep rate was determined by imaging the remanent state of the arrays of dots after applying one field pulse up to the intensity where half of the magnetization was reversed. We observe a clear increase in the coercive field, both with increasing field sweep rate and with decreasing dot size. This is in agreement with the expected increase in the anisotropy field due to a reduction in dot size. For the smaller dots, the coercive field at high sweep rate is, within the error bars, equal to the anisotropy field, which is the maximum coercive field expected for reversal by coherent rotation. Our data are not sufficient to establish for sure which model is suitable to describe the dynamic coercive field. However, if we assume that the models are valid, the fitting provides an estimation for the activation volume that can be compared to the value given by the aftereffect measurements. The moving DW model is able to fit our data with an activation volume of $3.50 \times 10^{-19} \text{ cm}^3$ for the $1 \mu\text{m}$ dots, and $2.70 \times 10^{-19} \text{ cm}^3$ for the

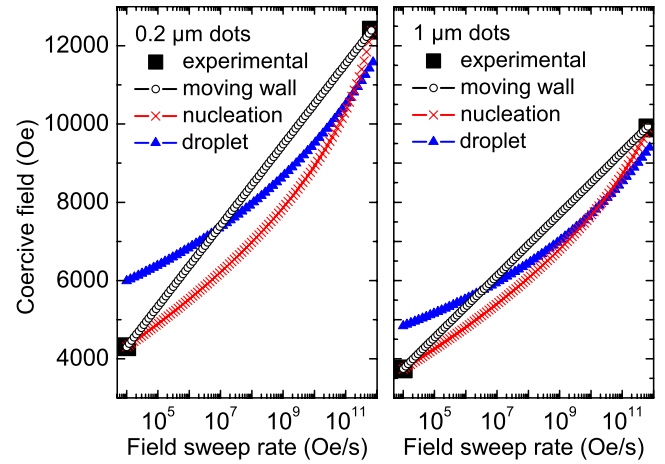


FIG. 8. (Color online) Experimental values and fitting of the coercive field as a function of field sweep rate for the $0.2 \mu\text{m}$ (left) and $1 \mu\text{m}$ (right) dots. From the fitting, $V_p^* = 3.50 \times 10^{-19}$, $V_n^* = 7.94 \times 10^{-19}$, and $\epsilon = 0.80$ for the $1 \mu\text{m}$ dots, and $V_p^* = 2.70 \times 10^{-19}$, $V_n^* = 7.28 \times 10^{-19}$, and $\epsilon = 0.93$ for the $0.2 \mu\text{m}$ dots.

$0.2 \mu\text{m}$ dots. The nucleation model is also able to fit our data with an activation volume of $7.94 \times 10^{-19} \text{ cm}^3$ for the $1 \mu\text{m}$ dots, and $7.28 \times 10^{-19} \text{ cm}^3$ for the $0.2 \mu\text{m}$ dots. If we assume a cylinder for the nucleation volume, its diameter is close to the exchange length. With the droplet model, it is not possible to perfectly fit our data. The best fit is obtained with $\epsilon = 0.80$ for the $1 \mu\text{m}$ dots, and $\epsilon = 0.93$ for the $0.2 \mu\text{m}$ dots.²⁰ The activation volume deduced from the moving DW model is consistently close to that deduced from aftereffect measurements, but is smaller than the one given by the nucleation model. From the moving DW model, we predict a linear variation of the coercive field H_c with the logarithm of the sweep rate \dot{H} as $H_c \sim (kT/V_p^* M_s) \log(\dot{H})$. As soon as the coercive field increases faster than linearly with respect to the logarithm of the sweep rate, one has to decrease the activation volume to fit the data with the moving wall model. Unfortunately, our experimental setup does not allow us to cover the midrange sweep rate to check the nonlinearity of this relation. We note that in the experiments of Moritz *et al.*, the increase was, indeed, nonlinear.⁴

For a domain, the ratio ρ between the DW velocity during the second pulse and the first pulse is given by $(d_2 - d_1)/(d_1 - d_{nuc})$. For a constant DW velocity during the first and second pulses, $\rho = 1$. From the analysis of eight dots with one magnetic domain in Figs. 5(a) and 5(c), and with an overestimated diameter $d_{nuc} = 22 \text{ nm}$ given by the droplet model, we find $\bar{\rho} = 0.39$ with a standard deviation of 0.27. The ratio between the DW velocity during the second pulse and the first pulse is within a 95% confidence interval $0.13 < \rho < 0.65$. Clearly, the DW velocity is not constant, but smaller during the second pulse than during the first one. We are all the more confident regarding the DW velocity as the overestimated value of d_{nuc} was given by the droplet model, which is not able to perfectly fit the dynamic coercive field (cf. Fig. 8). Hence, we conclude that the wall velocity at a nucleation center is larger than in the rest of the sample. This is opposite to what was observed in an exchange-biased soft

layer that was magnetized in-plane.¹⁸ However, from the expression of the wall velocity given in Ref. 19 it is expected that the propagation increases if the magnetic anisotropy decreases. Since there are always inhomogeneities in the sample properties, nucleation occurs preferentially at places where anisotropy is lower because the energy barrier is reduced, thereby explaining why wall velocity is larger at these locations.

In summary, we have studied magnetic reversal of patterned dots using short field pulses and MFM. For the 1 μm dots, we observe at moderate magnetic fields a partial reversal after one field pulse, which may be explained within a nucleation-propagation reversal mechanism. After one field pulse, the 0.2 μm dots were either not affected or completely reversed. The MFM images were interpreted in terms of magnetic aftereffects and a dynamic coercive field. We then

applied several models to estimate an upper limit for the nucleation volume. A better agreement was obtained with the nucleation model, leading to a cylindrical volume with a diameter that is close to the exchange length, but all models tested yield a nucleation volume of the same order of magnitude. We, therefore, conclude that the size of the observed domains is mainly due to domain wall propagation and that wall velocity is higher around nucleation centers.

ACKNOWLEDGMENTS

The authors thank A. Derory for the SQUID measurements, V. Da Costa for his support in imaging the magnetic domains, M. Acosta for the sample preparation, and M. Bowen for reading the manuscript.

-
- ¹J. Pommier, P. Meyer, G. Péniard, J. Ferré, P. Bruno, and D. Renard, *Phys. Rev. Lett.* **65**, 2054 (1990).
- ²Kwang-Su Ryu, Kyeong-Dong Lee, Sug-Bong Choe, and Sung-Chul Shin, *J. Appl. Phys.* **95**, 7306 (2004).
- ³B. Raquet, M. D. Ortega, M. Goiran, A. R. Fert, J. P. Redoules, R. Mamy, J.-C. Ousset, A. Sdaq, and A. Khmou, *J. Magn. Magn. Mater.* **150**, L5 (1995).
- ⁴J. Moritz, B. Dieny, J.-P. Nozières, Y. Pennec, J. Camarero, and S. Pizzini, *Phys. Rev. B* **71**, 100402(R) (2005); J. Moritz, Ph.D. thesis, Université Joseph Fourier, 2003.
- ⁵M. P. Sharrock, *J. Appl. Phys.* **76**, 6413 (1994).
- ⁶K. Mackay, M. Bonfim, D. Givord, and A. Fontaine, *J. Appl. Phys.* **87**, 1996 (2000).
- ⁷W. B. Pearson, *Handbook of Lattice Spacings and Structure of Metals and Alloys* (Pergamon, New York, 1964).
- ⁸M. Maret, M.-C. Cadeville, R. Poinot, A. Herr, E. Beaurepaire, and C. Monier, *J. Magn. Magn. Mater.* **166**, 45 (1997).
- ⁹P. W. Rooney, A. L. Shapiro, M. Q. Tran, and F. Hellman, *Phys. Rev. Lett.* **75**, 1843 (1995).
- ¹⁰P. Bruno, G. Bayreuther, P. Beauvillain, C. Chappert, G. Lugert, D. Renard, J.-P. Renard, and J. Seiden, *J. Appl. Phys.* **68**, 5759 (1990).
- ¹¹J. Valentin, Th. Kleinfeld, and D. Weller, *J. Phys. D* **29**, 1111 (1996).
- ¹²C. Raeder, Ph.D. thesis, Duisburg-Essen University, 2006.
- ¹³J. Ferré, V. Repain, J.-P. Jamet, A. Mougin, V. Mathet, C. Chappert, and H. Bernas, *Phys. Status Solidi A* **201**, 1386 (2004).
- ¹⁴M. Labrune, S. Andrieu, F. Rio, and P. Bernstein, *J. Magn. Magn. Mater.* **80**, 211 (1989).
- ¹⁵A. Kirilyuk, J. Ferré, J. Pommier, and D. Renard, *J. Magn. Magn. Mater.* **121**, 536 (1993).
- ¹⁶J.-P. Jamet, S. Lemerle, P. Meyer, J. Ferré, B. Bartenlian, N. Bardou, C. Chappert, P. Veillet, F. Rousseaux, D. Decanini, and H. Launois, *Phys. Rev. B* **57**, 14320 (1998).
- ¹⁷V. Harzer, Ph.D. thesis, RWTH Aachen, 1993.
- ¹⁸K. Fukumoto, W. Kuch, J. Vogel, F. Romanens, S. Pizzini, J. Camarero, M. Bonfim, and J. Kirschner, *Phys. Rev. Lett.* **96**, 097204 (2006).
- ¹⁹A. Mougin, M. Cormier, J. P. Adam, P. J. Metaxas, and J. Ferré, *Europhys. Lett.* **78**, 57007 (2007).
- ²⁰Nucleation takes place on defects where the effective anisotropy is reduced on average by a factor ϵ . With $\epsilon=0.8$, $d_{nuc}=20$ nm. The value $d_{nuc}=22$ nm is an upper value calculated with the measured effective anisotropy.